J|A|C|S
ARTICLES
Published on Web 02/09/2005

2,6-Diarylnaphtho[1,8-*bc*:5,4-*b′c′*]dithiophenes as New High-Performance Semiconductors for Organic Field-Effect Transistors

Kazuo Takimiya,*,† Yoshihito Kunugi,‡ Yuta Toyoshima,‡ and Tetsuo Otsubo†

Contribution from the Department of Applied Chemistry, Graduate School of Engineering, Hiroshima University, 1-4-1 Kagamiyama, Higashi-Hiroshima 739-8527, Japan and Faculty of Integrated Arts and Sciences, Hiroshima University, 1-7-1 Kagamiyama, Higashi-Hiroshima 739-8521, Japan

Received October 30, 2004; E-mail: ktakimi@hiroshima-u.ac.jp

Abstract: A series of 2,6-diaryl-substituted naphtho[1,8-*bc*:5,4-*b′c′*]dithiophene derivatives **2**−**6**, whose aryl groups include 5-hexyl-2-thienyl, 2,2′-bithiophen-5-yl, phenyl, 2-naphthyl, and 4-biphenylyl, was synthesized by the palladium-catalyzed Suzuki−Miyaura coupling and utilized as active layers of organic field-effect transistors (OFETs). All devices fabricated using vapor-deposited thin films of these compounds showed typical *p*-type FET characteristics. The mobilities are relatively good and widely range from 10^{-4} to 10^{-1} $cm^2\ V^{-1}\ s^{-1}$, depending on the substituent groups. Among them, the mobilities of the devices using films of **3**−**5** tend to increase with the increasing temperature of the Si/SiO_2 substrate during film deposition. In particular, the device based on the naphthyl derivative **5**, when fabricated at 140 °C, marked a high mobility of 0.11 $cm^2\ V^{-1}\ s^{-1}$ with an on/off ratio of 10^5, which is a top class of performance among organic thin-film transistors. Studies of X-ray diffractograms (XRDs) have revealed that the film of **4** and **5** is composed of two kinds of crystal grains with different phases, so-called "single-crystal phase" and "thin film phase", and that the proportion of the thin film phase increases with an increase of the substrate temperature. In the thin film phase the assembled molecules stand nearly upright on the substrate in such a way as to be favorable to carrier migration.

Introduction

In the past decade organic field-effect transistors (OFETs) have achieved remarkable progress by optimizing the fabrication of transistor devices and/or developing new organic semiconductors.[1] Device improvements have been exclusively conducted using superior semiconductors, such as pentacene,[2] oligothiophenes,[3] and regioregular polythiophenes,[4] but it seems that the improved performances of these devices nearly reach individual upper limits as far as the mobilities are concerned.[1] On the other hand, synthetic challenges to new organic semiconductors are still promising by virtue of the fact that versatile molecular systems have recently been found, which involve substituted pentacenes,[5] thienylene−phenylene cooligomers,[6] oligoselenophenes,[7] anthracene oligomers,[8] thiophene-containing acene-type compounds,[9] oligothienylenevinylenes,[10] benzo[1,2-*b*:4,5-*b′*]dichalcogenophenes,[11] carbazole derivatives,[12] and tetrathiafulvalene derivatives.[13]

In search of good semiconductors fused or extended heteroarenes are recognized as one of the most promising molecular systems.[1,3,9] As a part of our efforts to explore novel heteroarenes possessing very intriguing structures and physical properties, we previously developed two isomeric naphtho[1,8-*bc*:4,5-*b′c′*]-dithiophene (*syn*-NDT) and naphtho[1,8-*bc*:5,4-*b′c′*]dithiophene

† Graduate School of Engineering.
‡ Faculty of Integrated Arts and Sciences.

(1) (a) Dimitrakopoulos, C. D.; Malenfant, R. L. *Adv. Mater*. **2002**, *14*, 99−117. (b) Katz, H. E.; Bao, Z.; Gilat. S. L. *Acc. Chem. Res*. **2001**, *34*, 359−369. (c) Katz, H. E. *J. Mater. Chem*. **1997**, *7*, 369−376. (d) Katz, H. E. *Chem. Mater*. **2004**, *16*, 4748−756.
(2) (a) Gundlach, D. J.; Lin, Y. Y.; Jackson, T. N.; Nelson, S. F.; Schlom, D. G. *IEEE Electron Device Lett*. **1997**, *18*, 87−89. (b) Lin, Y. Y.; Gundlach, D. J.; Nelson, S. F.; Jackson, T. N. *IEEE Electron Device Lett*. **1997**, *18*, 606−608. (c) Lin, Y. Y.; Gundlach, D. J.; Nelson, S. F.; Jackson, T. N. *IEEE Trans. Electron Devices* **1997**, *45*, 1325−1331. (d) Knipp, D.; Street, R. A.; Völkel, A.; Ho, J. *J. Appl. Phys*. **2003**, *93*, 347−355.
(3) (a) Garnier, F.; Yassar, A.; Hajlaoui, R.; Horowitz, G.; Deloffre, F.; Servet, B.; Ries, S.; Alnot, P. *J. Am. Chem. Soc*. **1993**, *115*, 8716−8721. (b) Servet, B.; Horowitz, G.; Ries, S.; Lagorsse, O.; Alnot, P.; Yassar, A.; Deloffre, F.; Srivastava, P.; Hajlaoui, R.; Lang. P.; Garnier, F. *Chem. Mater*. **1994**, *6*, 1809−1815. (c) Hajlaoui, R.; Horowitz, G.; Garnier, F.; Arce-Brouchet, A.; Laigre, L.; Kassmi, A. El; Demanze, F.; Kouki, F. *Adv. Mater*. **1997**, *9*, 389−391. (d) Hajlaoui, R.; Fichou, D.; Horowitz, G.; Nessakh, B.; Constant, M.; Garnier, F. *Adv. Mater*. **1997**, *9*, 557−561. (e) Katz, H. E.; Torsi, L.; Dodabalapur, A. *Chem. Mater*. **1995**, *7*, 2235−2237. (f) Katz, H. E.; Dodabalapur, A.; Torsi, L.; Elder, D. *Chem. Mater*. **1995**, *7*, 2238−2240. (g) Katz, H. E.; Lovinger, A. J.; Laquindanum, J. G. *Chem. Mater*. **1998**, *10*, 457−459. (h) Katz, H. E.; Laquindanum, J. G.; Lovinger, A. J. *Chem. Mater*. **1998**, *10*, 633−638. (i) Facchetti, A.; Yoon, M.-H.; Stern, C. L.; Katz, H. E.; Marks, T. J. *Angew. Chem., Int. Ed*. **2003**, *42*, 3900−3903. (j) Facchetti, A.; Mushrush, M.; Katz, H. E.; Marks, T. J. *Adv. Mater*. **2003**, *15*, 33−38. (k) Halik, M.; Klauk, H.; Zschieschang, U.; Schmid, G.; Ponomarenko, S.; Kirchmeyer, S.; Weber, W. *Adv. Mater*. **2003**, *15*, 917−922. (l) Murphy, A. R.; Fréchet, J. M. J.; Chang, P.; Lee, J.; Subramanian, V. *J. Am. Chem. Soc*. **2004**, *126*, 1596−1597. (m) Facchetti, A.; Mushrush, M.; Yoon, M.-H.; Hutchison, G. R.; Ratner, M. A.; Marks, T. J. *J. Am. Chem. Soc*. **2004**, *126*, 13859−13874.
(4) (a) Sirringhaus, H.; Brown, P. J.; Friend, R. H.; Nielsen, M. M.; Bechgaard, K.; Langeveld-Voss, B. M. W.; Spiering, A. J. H.; Janssen, R. A. J.; Meijer, E. W.; Herwig, P.; de Leeuw, D. M. *Nature* **1999**, *401*, 685−688. (b) Guangming, W.; Swensen, J.; Moses, D.; Heeger, A. J. *J. Appl. Phys*. **2003**, *93*, 6137−6141. (c) Ong, B. S.; Wu, Y.; Liu, P.; Gardner, S. *J. Am. Chem. Soc*. **2004**, *126*, 3378−3379. (d) Chang, J.-F.; Sun, B.; Breiby, D. W.; Nielsen, M. M.; Solling, T. I.; Giles, M.; McCulloch, I.; Sirringhaus, H. *Chem. Mater*. **2004**, *16*, 4772−4776.

(*anti*-NDT) and their dithienyl derivatives,[14,15] which served as good donor components for molecular-based conductors and conducting polymers. These fused heteroarenes are formally isoelectronic with pyrene, but their aromatic characters are greatly reduced by loss of Kekulé benzene rings in the skeletons owing to the introduction of two thiophene rings. As a result, the HOMO energy levels of these π-systems are markedly raised whereas the LUMO energy levels are lowered. It is thus expected that the NDT systems might possess semiconducting character. In a preliminary experiment we found that the device fabricated with *anti*-di(2-thienyl)naphthodithiophenes (*anti*-DTh−NDT **1**) showed *p*-type FET characteristics while that with the syn isomer (*syn*-DTh−NDT**)** did not respond.[16] Although the mobility is not so high (10^{-4} cm^2 V^{-1} s^{-1}), this result suggests that the *anti*-NDT system is a potential prototype for a new superior semiconductor, and its chemical modifications are worth examining. In this article we report the synthesis, electrochemical and spectroscopic properties, and solid-state structures of various *anti*-NDT derivatives **2**−**6** bearing 5-hexyl-2-thienyl, 2,2′-bithiophen-5-yl, phenyl, 2-naphthyl, and 4-biphenylyl substituents at the 2- and 6-positions as well as their FET characteristics, Chart 1.

Chart 1

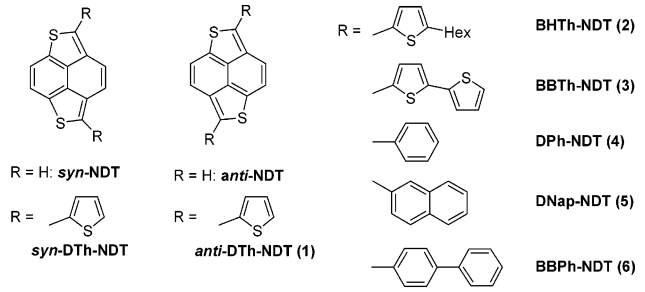

Experimental Section

Synthesis. 2,6-Diaryl-NDTs (**2**−**6**) were synthesized according to Scheme 1 in which the palladium-catalyzed Suzuki−Miyaura coupling was employed as a key step to introduce various aryl substituents.[17]

Scheme 1. Synthesis of 2,6-Diaryl-NDT Derivatives

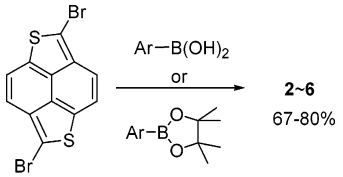

7

Thus, readily available aryl boronic acids or aryl boronic acid pinacol esters[18] were reacted with 2,6-dibromonaphtho[1,8-*bc*:5,4-*b′c′*]dithiophene (**7**)[14b,c] to give the corresponding 2,6-diaryl-NDTs (**2**−**6**) in 67−80% yields after purification (see Supporting Information for details). All these new compounds were characterized by ^{1}H NMR spectra, mass spectra, and elemental analysis, except the 4-biphenylyl derivative (**6**), which was too insoluble to measure its ^{1}H NMR spectrum. In addition, the molecular structures of the diphenyl (**4**), di(2-naphthyl) (**5**), and bis(4-biphenylyl) derivatives (**6**) were fully elucidated by X-ray crystallographic analyses.

X-ray Diffraction Measurement. X-ray diffractions of organic thin films deposited on the Si/SiO$_2$ substrate were obtained with a Maxscience M18XHF diffractometer with a Cu Kα source (λ = 1.541 Å) in air. Single crystals of **4**−**6** suitable for X-ray structural analyses were obtained by recrystallization or vacuum sublimation[19] and analyzed with a Rigaku AFC7R four-circle diffractometer (Mo Kα radiation, λ = 0.710 69 Å, graphite monochromator, $2\theta_{max}$ = 55.0°) or Rigaku Rapid-S imaging plate diffractometer (Mo Kα radiation, λ = 0.710 69 Å, graphite monochromator, $2\theta_{max}$ = 55.0°). The structures were solved by direct methods (SIR92)[20] and refined by full-matrix least-squares on $|F|^2$ (SHELEX 97).[21] Table 1 summarizes the structural parameters.

Device Preparation. OFETs were fabricated in a top-contact manner as follows. A thin film (50 nm thick) of the NDT derivatives as an active layer was vacuum-deposited on heavily doped n^+-Si (100) wafers with a 230 nm thermally grown SiO$_2$, and successively, Au films (80 nm) as drain and source electrodes were deposited on the organic layer through a shadow mask. For a typical device the drain-source channel length (L) and width (W) are 50 μm and 1.5 mm, respectively. Characteristics of a drain current (I_{DS}) versus drain voltage (V_{DS}) of the OFET devices were measured under vacuum with an ADVANTEST R6245 power supply. The field-effect mobilities (μ_{FET}) were calculated in the saturation regime of the I_{DS} using the equation $I_{DS} = (WC_i/2L)\mu_{FET}(V_G - V_T)^2$, where C_i is the capacitance of the SiO$_2$ insulator (C_i = 1.50 × 10^{-8} Fcm^{-2}) and V_G and V_T are the gate and threshold voltages, respectively. The film deposition was conducted at different substrate temperatures (T_{sub}) in order to examine the dependence of mobility or morphology on T_{sub}.

(5) (a) Meng, H.; Bendikov, M.; Mitchell, G.; Helgeson, R.; Wudl, F.; Bao, Z.; Siegrist, T.; Kloc, C.; Chen, C. H. *Adv. Mater.* **2003**, *15*, 1090−1093. (b) Sheraw, C. D.; Jackson, T. N.; Eaton, D. L.; Anthony, J. E. *Adv. Mater.* **2003**, *15*, 2009−2011. (c) Sakamoto, Y.; Suzuki, T.; Kobayashi, M.; Gao, Y.; Fukai, Y.; Inoue, Y.; Sato, F.; Tokito, S. *J. Am. Chem. Soc.* **2004**, *126*, 8138−8140.

(6) (a) Hong, X. M.; Katz, H. E.; Lovinger, A. J.; Wang, B.-C.; Raghavachari, K. *Chem. Mater.* **2001**, *13*, 4686−4691. (b) Meng, H.; Bao, Z.; Lovinger, A. J.; Wang, B.-C.; Mujsce, A. M. *J. Am. Chem. Soc.* **2001**, *123*, 9214−9215. (c) Ichikawa, M.; Yanagi, H.; Shimizu, Y.; Hotta, S.; Suganuma, N.; Koyama, T.; Taniguchi, Y. *Adv. Mater.* **2002**, *14*, 1272−1275. (d) Mushrush, M.; Facchetti, A.; Lefenfeld, M.; Katz, H. E.; Marks, T. J. *J. Am. Chem. Soc.* **2003**, *125*, 9414−9423. (e) Meng, H.; Zheng, J.; Lovinger, A. J.; Wang, B.-C.; Van Patten, P. G.; Bao, Z. *Chem. Mater.* **2003**, *15*, 1778−1787. (f) Facchetti, A.; Letizia, J.; Yoon, M.-H.; Mushrush, M.; Katz, H. E.; Marks, T. J. *Chem. Mater.* **2004**, *16*, 4715−4727.

(7) Kunugi, Y.; Takimiya, K.; Yamane, K.; Yamashita, K.; Aso, Y.; Otsubo, T. *Chem. Mater.* **2003**, *15*, 6−7.

(8) Ito, K.; Suzuki, T.; Sakamoto, Y.; Kubota, D.; Inoue, Y.; Sato, F.; Tokito, S. *Angew. Chem., Int. Ed.* **2003**, *42*, 1159−1162.

(9) (a) Laquindanum, G. L.; Katz, H. E.; Lovinger, A. J.; Dodabalapur, A. *Adv. Mater.* **1997**, *9*, 36−39. (b) Li, X.-C.; Sirringhaus, H.; Garnier, F.; Holmes, A. B.; Moratti, S. C.; Feeder, N.; Clegg, W.; Teat, S. J.; Friend, R. H. *J. Am. Chem. Soc.* **1998**, *120*, 2206−2207. (c) Sirringhaus, H.; Friend, R. H.; Wang, C.; Leuningerb, J.; Müllen, K. *J. Mater. Chem.* **1999**, *9*, 2095−2101. (d) Laquindanum, J. G.; Katz, H. E.; Lovinger, A. J. *J. Am. Chem. Soc.* **1998**, *120*, 664−672.

(10) Videlot, C.; Ackermann, J.; Blanchard, P.; Raimundo, J.-M.; Frère, P.; Allain, M.; Bettignies, R.; Levillain, E.; Roncali, J. *Adv. Mater.* **2003**, *15*, 306−310.

(11) Takimiya, K.; Kunugi, Y.; Konda, Y.; Niihara, N.; Otsubo, T. *J. Am. Chem. Soc.* **2004**, *126*, 5084−5085.

(12) (a) Wakim, S.; Bouchard, J.; Simard, M.; Drolet, N.; Tao, Y.; Leclerc, M. *Chem. Mater.* **2004**, *16*, 4386−4388. (b) Morin, J.-F.; Drolet, N.; Tao, Y.; Leclerc, M. *Chem. Mater.* **2004**, *16*, 4619−4626.

(13) (a) Xue, J.; Forrest, S. R. *Appl. Phys. Lett.* **2001**, *79*, 3714−3716. (b) Takada, M.; Graaf, H.; Yamashita, Y.; Tada, H. *Jpn. J. Appl. Phys.* **2002**, *41*, L4−L6. (c) Mas-Torrent, M.; Durkut, M.; Hadley, P.; Ribas, X.; Rovira C. *J. Am. Chem. Soc.* **2004**, *126*, 984−985. (d) Mas-Torrent, M.; Hadley, P.; Bromley, S. T.; Ribas, X.; Tarrés, J.; Mas, M.; Molins, E.; Veciana, J.; Rovira, C. *J. Am. Chem. Soc.* **2004**, *126*, 8546−8553.

(14) (a) Takimiya, K.; Yashiki, Y.; Aso, Y.; Otsubo, T.; Ogura, F. *Chem. Lett.* **1993**, 365−368. (b) Takimiya, K.; Otsubo, T.; Ogura, F. *J. Chem. Soc., Chem. Commun.* **1994**, 1859−1860. (c) Takimiya, K.; Kato, K.; Aso, Y.; Ogura, F.; Otsubo, T. *Bull. Chem. Soc. Jpn.* **2002**, *75*, 1795−1805.

(15) Casado, J.; Quirante, J. J.; Hernández, V.; Navarrete, J. T. L.; Takimiya, K.; Otsubo, T. *J. Phys. Chem. B* **2004**, *108*, 7611−7619.

(16) Kunugi, Y.; Takimiya, K.; Yamashita, K.; Aso, Y.; Otsubo, T. *Chem. Lett.* **2002**, 958−959.

(17) Miyaura, N.; Suzuki, A. *Chem. Rev.* **1995**, *95*, 2457−2483.

(18) Andersen, M. W.; Hildbrandt, B.; Köster, G.; Hoffmann, W. *Chem. Ber.* **1989**, *122*, 1777−1782.

(19) Crystals of **2** and **3** suitable for X-ray analysis could not be obtained by recrystallization or vacuum sublimation.

(20) Altomare, A.; Burla, M. C.; Camalli, M.; Cascarano, M.; Giacovazzo, C.; Guagliardi, A.; Polidori, G. *J. Appl. Crystallogr.* **1994**, *27*, 435−436.

(21) Sheldrick, G. M. *Programs for the Refinement of Crystal Structures*; University of Gottingen: Gottingen, Germany, 1997.

Table 1. Crystal Data for **4**−**6**

	4	5	6
formula	$C_{24}H_{14}S_2$	$C_{32}H_{18}S_2$	$C_{36}H_{22}S_2$
formula weight	366.50	466.61	518.69
method of crystal growth	recrystallization from chloroform	vacuum sublimation	vacuum sublimation
color and shape of crystal	red prism	red plate	red prism
crystal dimensions/mm^3	0.25 × 0.25 × 0.12	0.50 × 0.20 × 0.02	0.12 × 0.10 × 0.10
instruments	Rigaku RAPID-S	Rigaku AFC7R	Rigaku AFC7R
type of data collection	IP	ω	$\omega - 2\theta$
crystal system	orthorhombic	orthorhombic	monoclinic
space group	*Pbca*	*Pbca*	$P2_1$
a/Å	7.3528(1)	7.264(3)	12.965(2)
b/Å	8.1884(1)	8.432(2)	7.620(2)
c/Å	28.6857(5)	36.215(7)	12.498(1)
β/deg			100.246(10)
V/Å3	1717.10(5)	2217(1)	1215.0(4)
temp/K	296	296	296
Z	4	4	2
reflections collected	2264	3626	3604
no. of data [$I > 2.0\sigma(I)$]	1651	1518	1928
R^a; $R_w{}^b$	0.065; 0.182	0.041; 0.154	0.040; 0.139
GOF	1.49	0.93	0.88

[a] $R = \Sigma\,(|F_o| - |F_c|)/\Sigma|F_o|$ for observed data. [b] $R_w = \{\Sigma\omega(F_o^2 - F_c^2)^2/\Sigma\omega(F_o^2)^2\}^{1/2}$ for all data.

Table 2. Electrochemical and Spectroscopic Properties of NDT Derivatives (**2**−**6**)

	CV[a]	UV−vis[b]		emission[b]	
compound	$E_{1/2}$/V	λ_{abs}/nm	ϵ	λ_{emis}/nm[d]	Φ^f
BHTh−NDT (**2**)	+ 0.06	532	34 000	584	0.14
BBTh−NDT (**3**)	+ 0.02	566	54 900	635[e]	0.01[g]
DPh−NDT (**4**)	+ 0.29	482	34 200	530	0.50
DNap−NDT (**5**)	+ 0.22	501	37 500	552	0.47
BBPh−NDT (**6**)	+ 0.25	500	c	557	0.32

[a] Cyclic voltammetry was recorded at 100 mV s^{-1} scan rate with Pt working and counter electrodes and Ag/AgCl reference electrode in dichloromethane solution containing 0.1 M tetrabutylammonium perchlorate. The obtained potentials were calibrated with the standard ferrocene/ferrocenium redox couple. [b] Measured in tetrahydrofuran. [c] Because of the poor solubility, the molar absorption coefficient cannot be determined. [d] Excited at 350 nm unless otherwise stated. [e] Excited at 560 nm. [f] Calculated based on quinine bisulfate in 0.5 M H_2SO_4 as a standard unless otherwise stated. [g] Calculated based on Rhodamine 101 as reference.

Other Instrumental Measurements. UV−vis and emission spectra in THF solution were recorded on a Shimadzu UV-3100 spectrophotometer and a Perkin Elmer LS45 luminescent spectrophotometer, respectively. Fluorescence quantum yield was comparatively determined using quinine bisulfate in 0.5 M H_2SO_4 or Rhodamine 101 in ethanol as standard.[22] Cyclic voltammograms were measured in dichloromethane containing 0.1 M tetrabutylammonium perchlorate at room temperature using a Hokuto Denko HA-301 potentiostat and a Hokuto Denko HB-104 function generator. The oxidation potentials were recorded against a Ag/AgCl reference electrode and were calibrated with the standard ferrocene/ferrocenium redox couple. AFM images of the evaporated thin films on Si/SiO_2 substrate were obtained by using a Shimadzu SPM-9500 microscope in air.

Results and Discussion

Electrochemical and Spectroscopic Properties. The oxidation potentials of the NDT derivatives measured by cyclic voltammetry together with the spectroscopic data are summarized in Table 2. The oxidation potentials of **2** and **3** bearing thienyl substituents (+0.06 and +0.02 V, respectively, vs Fc/Fc^+) are lower by ca. 0.2 V than those of **4**−**6** with phenyl or naphthyl substituents. This means that the highest occupied molecular orbital (HOMO) of the *anti*-NDT core is more effectively elevated by π-conjugation with thienyl substituents than with phenyl and naphthyl substituents.

Absorption spectra of **2**−**6** also provide information on the extent of π-conjugation between the NDT core and the substituents. Compared to that of the parent *anti*-NDT (λ_{max} = 411 nm),[14b,14c] the $\pi-\pi^*$ transitions of **2** (λ_{max} = 532 nm) and **3** (λ_{max} = 566 nm) show large bathochromic shifts. This corroborates effective π-conjugation between the NDT core and the thienyl substituents, as indicated by the above electrochemical study. On the other hand, the $\pi-\pi^*$ transition of the phenyl derivative **4** (λ_{max} = 482 nm) shows a less pronounced bathochromic shift than that of **2**, evidently supporting that phenyl conjugation is not as effective as thienyl conjugation. Extension of the π-system from phenyl to naphthyl substitution (**5**) or to biphenyl substitution (**6**) causes a bathochromic shift by ca. 20 nm, which is much smaller than that (34 nm) from thienyl to bithiophenyl substitution. In accordance with the shifts of the absorption bands, the emission bands of **2**−**6** appear in the much longer wavelength region (λ_{max} = 530−635 nm) than that of the parent *anti*-NDT (λ_{max} = 427 nm).[14b,c] The fluorescence quantum yields of **2** (Φ^f 0.14) and **3** (Φ^f 0.01) bearing thienyl substituents are more markedly reduced than those (Φ^f 0.32−0.50) of **4**−**6** bearing phenyl or naphthyl substituents. This suggests that the photoexcited state is efficiently quenched by interactions involved with the sulfur atoms of the attached heterocyclic rings.

X-ray Structural Analysis. Figure 1 shows molecular structures of **4**−**6**. The central NDT cores of these compounds are almost flat, but the aryl substituents are not in the same plane, as expected from the above electrochemical and spectroscopic studies. Mean torsion angles between the NDT core and the aryl substituents are 27.3°, 30.5°, and 24.5° for **4**, **5**, and **6**, respectively. These large torsion angles are in sharp contrast to that of DTh−NDT (**1**, 14.7°) previously analyzed.[14c] A systematic study of FET devices using these compounds would thus give some information on how molecular deviation from coplanarity influences their semiconducting properties.

The crystal structures of the three derivatives are shown in Figure 2. The phenyl and naphthyl derivatives **4** and **5** have basically the same molecular packings in which the molecules

(22) Eaton, D. F. *Pure Appl. Chem.* **1998**, *60*, 1107−1114.

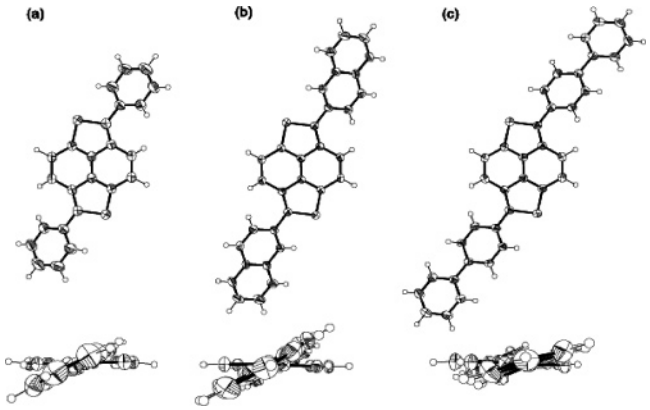

Figure 1. Molecular structures of (a) DPh-NDT (**4**), (b) DNap-NDT (**5**), and (c) BBPh-NDT (**6**): (top) top view of the molecule; (bottom) side view along the molecular long axis.

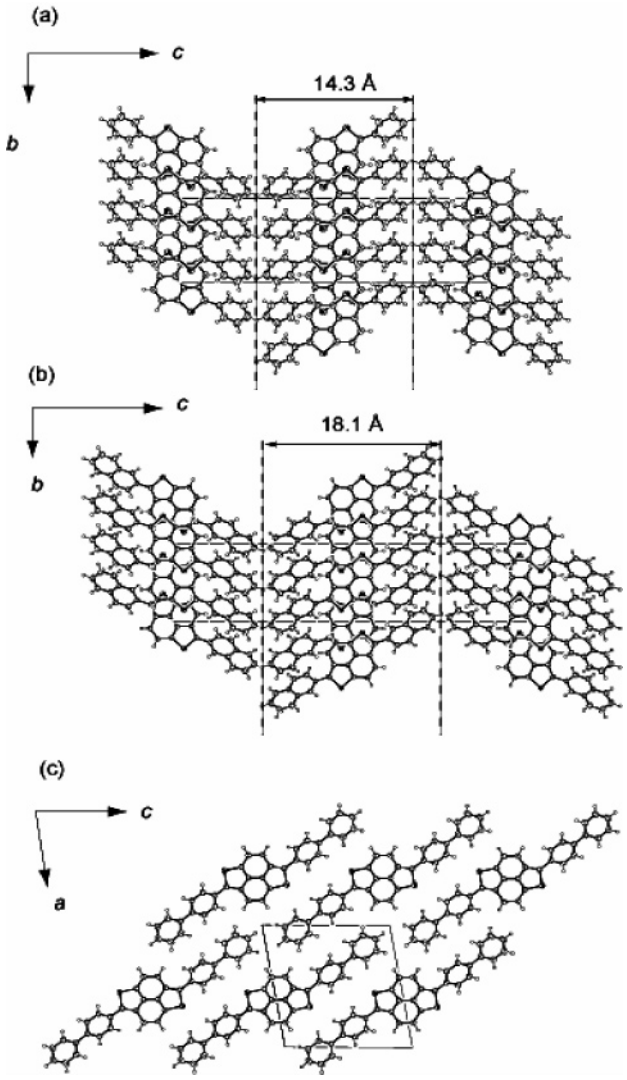

Figure 2. Crystal structures of **4**−**6**: (a and b): *a*-axis projection of **4** and **5**, respectively, representing "layer-by-layer" structure along the *c*-axis direction. The half of the *c*-axis corresponds to the layer width. (c *b*-Axis projection of **6**. For clarity, only one sheetlike array of molecules ($0.5 < b < 1.0$) is depicted.

are crystallized in a "layer-by-layer" structure. The unit cell contains two layers along the *c*-axis direction, and thus one-half of the *c*-axis length, 14.3 and 18.1 Å for **4** and **5**,

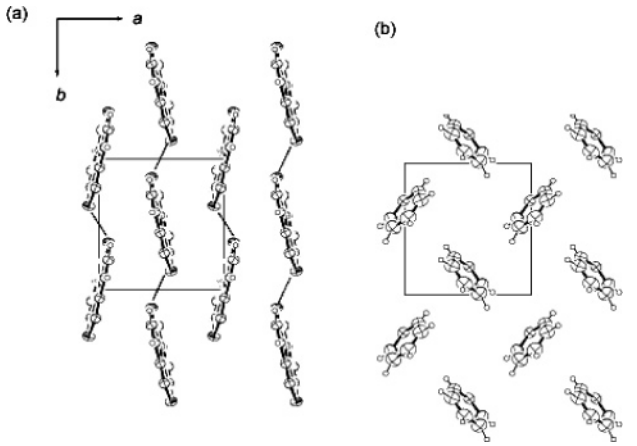

Figure 3. Packing diagram of **4** in the molecular layer. For clarity, the NDT part and phenyl substituents are depicted separately in a and b, respectively, and their superimposition gives a *c*-axis projection. The dotted line represents short S−S intermolecular contacts (3.35 Å) through the sulfur atoms in the NDT core.

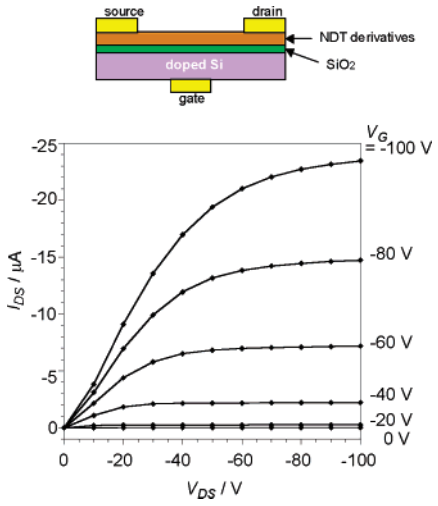

Figure 4. Drain-source current (I_{DS}) versus drain-source voltage (V_{DS}) characteristic for **4** (T_{sub} = 60 °C) and schematic picture of an OFET device.

respectively, corresponds to the width of each layer. In the layer the packing arrangement is somewhat different from the typical herringbone type, especially at the central NDT core. Figure 3a shows the arrangement of the NDT cores in the crystal structure of DPh−NDT (**4**); neither intermolecular "face-to-face" nor "face-to-edge" interaction of π-orbitals is observed, but one-dimensional ribbonlike interactive arrays exist through S−S contacts (3.35 Å) shorter than the sum of van der Waals radius. On the other hand, the phenyl subunits take on a herringbone-type of arrangement, as shown in Figure 3b. The crystal arrangements of the NDT core and the naphthyl subunits of DNap−NDT (**5**) are essentially the same as those of DPh−NDT (**4**).

In contrast to the crystal structures of **4** and **5**, BBPh−NDT (**6**) does not crystallize in the "layer-by-layer" molecular arrangement (Figure 2c). The molecules are loosely packed to form a sheetlike array in the *ac* plane in which no short S−S contact is observed. The molecular sheets are piled up in the *b*-axis direction, but neither π-stack interaction nor intermolecular S−S interaction exist in this direction.

OFET Device Characteristics. All the OFET devices using the NDT derivatives showed *p*-type transistor responses; the

Table 3. Field-Effect Mobility and On/Off Ratio for Transistors of **2**−**6** Prepared at Different Substrate Temperature (T_{sub})

	T_{sub} = rt (25 °C)		T_{sub} = 60 °C		T_{sub} = 100 °C		T_{sub} = 140 °C	
compound	mobility/cm^2 V^{-1} s^{-1}	on/off ratio	mobility/cm^2 V^{-1} s^{-1}	on/off ratio	mobility/cm^2 V^{-1} s^{-1}	on/off ratio	mobility/cm^2 V^{-1} s^{-1}	on/off ratio
BHTh−NDT (**2**)	1.0×10^{-4}	<10	no FET		no FET			
BBTh−NDT (**3**)	6.0×10^{-3}	600	4.1×10^{-2}	10^3	3.8×10^{-2}	10^3		
DPh−NDT (**4**)	6.1×10^{-3}	10^3	1.7×10^{-2}	10^4	5.7×10^{-2}	3×10^4	5.2×10^{-2}	10^5
DNap−NDT (**5**)	5.3×10^{-3}	4×10^3	5.3×10^{-2}	6×10^4	1.0×10^{-1}	10^5	1.1×10^{-1}	10^5
BBPh−NDT (**6**)	2.9×10^{-2}	2×10^4	3.6×10^{-2}	3×10^4	2.9×10^{-2}	4×10^4		

source-drain current (I_{DS}) scales up as the gate voltage (V_G) becomes more negative. As an example, I_{DS} versus V_{DS} curves for the DPh−NDT (**4**) film deposited at T_{sub} = 60 °C is shown in Figure 4. Field-effect mobility (μ_{FET}) was determined using the saturation regime and an on/off ratio of the I_{DS} between V_G = 0 and −100 V. The FET performances of all the NDT compounds are summarized in Table 3.

Although introduction of long alkyl chains at the longitudinal ends of semiconducting molecules has been proved to be a promising approach to improve thin film OFET characteristics,[1,3,6b,e] a comparison of the FET characteristics of BHTh−NDT (**2**) (μ_{FET} 1.0×10^{-4} cm^2 V^{-1} s^{-1} and on/off ratio < 10) with those of DTh−NDT (**1**) (μ_{FET} 3×10^{-4} cm^2 V^{-1} s^{-1} and on/off ratio 30)[16] indicates that the *n*-hexyl groups are, in our case, of no use for improvement of OFET performance. On the other hand, extension of π-conjugation from thienyl to bithiophenyl substitution quite effectively improves not only the mobility but also the on/off ratio. The device of BBTh−NDT (**3**) fabricated at T_{sub} = rt showed an enhanced mobility (μ_{FET} 6.0×10^{-3} cm^2 V^{-1} s^{-1}) and on/off ratio (600), both of which are 20 times higher than those of DTh−NDT (**1**). An increase of the substrate temperature T_{sub} to 60 °C or more resulted in an enhancement of the mobility by 1 order of magnitude.

Replacement of the thienyl groups of **1** with phenyl groups also serves to improve FET characteristics. An OFET device based on DPh−NDT (**4**) showed nearly the same high mobility (μ_{FET} 6.1×10^{-3} cm^2 V^{-1} s^{-1}) with an on/off ratio of 10^3 at T_{sub} = rt as BBTh−NDT (**3**). In a similar manner, mobility and on/off ratio are enhanced by 1 order of magnitude with an increase of T_{sub}. Furthermore, on/off ratios of DPh−NDT (**4**) based OFETs are always higher than those of BBTh−NDT (**3**) based OFETs for all T_{sub}. This is attributed to the lower HOMO of DPh−NDT (**4**) than that of BBTh−NDT (**3**) as discussed above, reducing the off current (I_{off}) of the devices.[6b,e,23] A more pronounced dependence of the FET characteristics on T_{sub} was observed for the device based on the naphthyl derivative **5**. The mobility (μ_{FET} 5.3×10^{-3} cm^2 V^{-1} s^{-1}) recorded at T_{sub} = rt was enhanced by 2 orders of magnitude to 1.0×10^{-1} cm^2 V^{-1} s^{-1} at T_{sub} = 100 °C and to 1.1×10^{-1} cm^2 V^{-1} s^{-1} at T_{sub} = 140 °C. The on/off ratio was also drastically improved from 10^3 to 10^5. This FET performance is of a top class among thin film organic semiconductors. The biphenyl derivative (**6**) also showed a good OFET characteristic of μ_{FET} = 2.9×10^{-2} cm^2 V^{-1} s^{-1} with an on/off ratio of 2×10^4 at T_{sub} = rt. However, the performance was not affected by elevation of the substrate temperature.

It should be worth noting that introduction of phenyl and 2-naphthyl substituents, though they are not allowed to fully conjugate with the NDT core, is very effective to induce the high FET performances of this system. This is in sharp contrast as preceding high-performance OFET materials such as pentacene[24] and sexithiophene[25] have completely or nearly planar molecular structures enabling extended π-conjugation over the whole molecules and two-dimensional electronic interactions in typical herringbone-type crystal structures.[26]

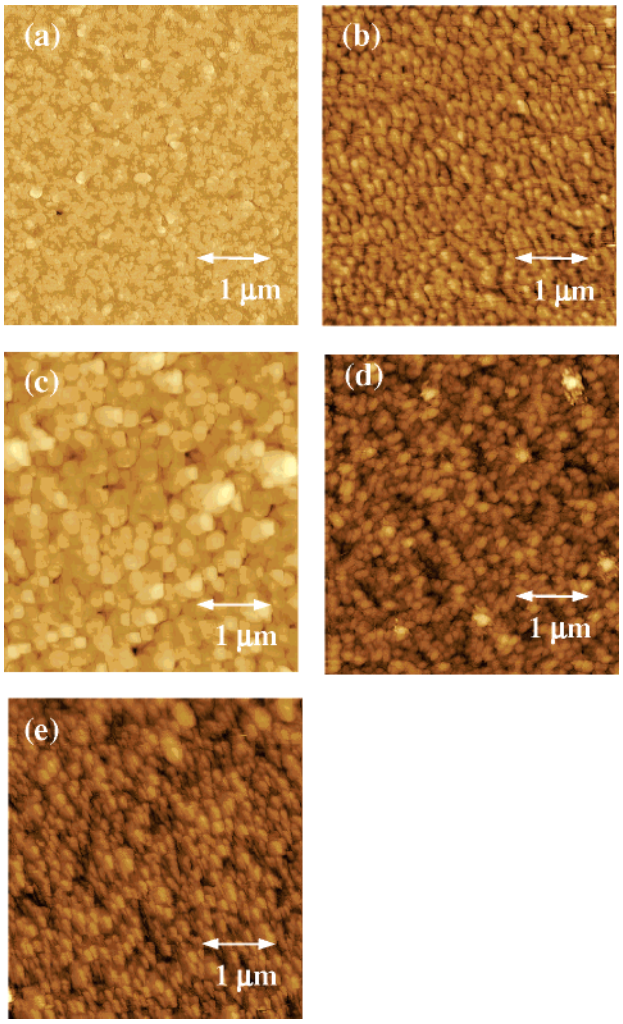

Figure 5. AFM images of thin films on Si/SiO$_2$ evaporated at T_{sub} = rt: (a) BHTh−NDT (**2**), (b) BBTh−NDT (**3**), (c) DPh−NDT (**4**), (d) DNap−NDT (**5**), and (e) BBPh−NDT (**6**).

Characterization of Thin Films. Figure 5 show AFM images of the evaporated thin films of the NDT derivatives (**2**−**6**) on

(23) Mohapatra, S.; Holmes, B. T.; Newman, C. R.; Prendergast, C. F.; Frisbie, C. D.; Ward, M. D. *Adv. Funct. Mater*. **2004**, *14*, 605−609.

(24) Cornil, J.; Calbert, J.-P.; Brédas, J.-L. *J. Am. Chem. Soc*. **2001**, *123*, 1250−1251.

(25) (a) Horowiz, G.; Bachet, B.; Yassar, A.; Lang, P.; Demanze, F.; Fave, J. L.; Garnier, F. *Chem. Mater*. **1995**, *7*, 1337−1341. (b) Siegrist, T.; Fleming, R. M.; Haddon, R. C.; Laudise, R. A.; Lovinger, A. J.; Katz, H. E.; Bridenbaugh, P.; Davis, D. D. *J. Mater. Res*. **1995**, *10*, 2170−2173.

(26) (a) Cornil, J.; Calbert, J.-P.; Beljonne, D.; Silbey, R.; Brédas, J.-L. *Adv. Mater*. **2000**, *12*, 978−983. (b) Bromley, S. T.; Mas-Torrent, M.; Hadley, P.; Rovira, C. *J. Am. Chem. Soc*. **2004**, *126*, 6544−6545.

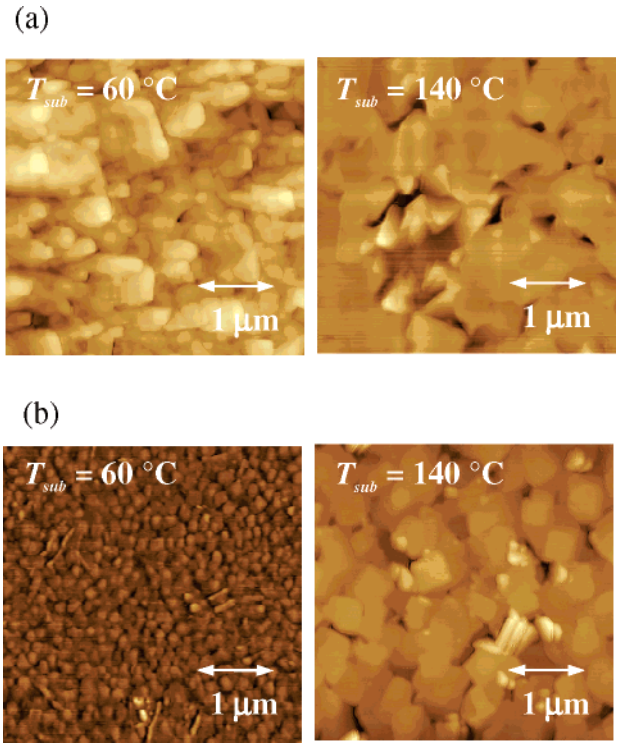

Figure 6. AFM images of thin films evaporated at T_{sub} = 60 and 140 °C: (a) DPh−NDT (**4**) and (b) DNap−NDT (**5**).

Si/SiO_2 substrate at T_{sub} = rt. The AFM images indicate that these films consist of small grains with sizes of ca. 0.01−0.2 μm. The grain sizes are not apparently related to the structures as well as the FET performances of the compounds. Concomitantly, the grain sizes of DPh−NDT (**4**) and DNap−NDT (**6**) (Figure 6) increase with increasing T_{sub} and become 0.5−1.0 μm at T_{sub} = 140 °C. Evidently, these morphological changes correlate closely with marked improvements in the FET characteristics of **4** and **5** at high substrate temperatures.

X-ray diffraction analyses of thin films give us information on the molecular arrangement in the crystal grains. As shown in Figure 7 the X-ray diffractograms (XRD) of thin films **2**−**6** consist of a series of sharply resolved peaks assignable to multiple (00*l*) reflections, indicating high quality for the thin films. Table 4 summarizes the calculated interlayer spacing (*d*) together with the molecular lengths (*l*)[24] and calculated tilt angle (θ_{tilt}) against the normal to the substrate (Figure 8).

The interlayer spacing (*d*) determined from the first-layer line of the XRD of **2** (Figure 7a) is 23.9 Å, which gives a tilt angle (θ_{tilt}) of 36°.[27] That is, the molecules of **2** in the thin film largely incline from the normal to the substrate, which makes intermolecular π-overlap as well as heteroatomic interactions less favorable. This accounts for the low mobility ($\sim 10^{-4}$ cm^2 V^{-1} s^{-1}) of the FET device fabricated with **2**. Figure 7b shows XRD of the thin film **3** consisting of well-resolved peaks with higher ordering. Its *d* spacing is determined to be 19.3 Å, which corresponds to a θ_{tilt} of 35°. A similar large inclined molecular arrangement (θ_{tilt} 35°) is estimated in the thin film of the 4-biphenylyl derivative (**6**). As shown in Figure 7e a series of multiple (00*l*) reflections observed in XRD, though there are

(27) Since the molecular structures of BHTh−NDT (**2**) and BBTh−NDT (**3**) are not obtained by X-ray structure analysis, the lengths of these molecules are estimated by MOPAC PM3 calculation.

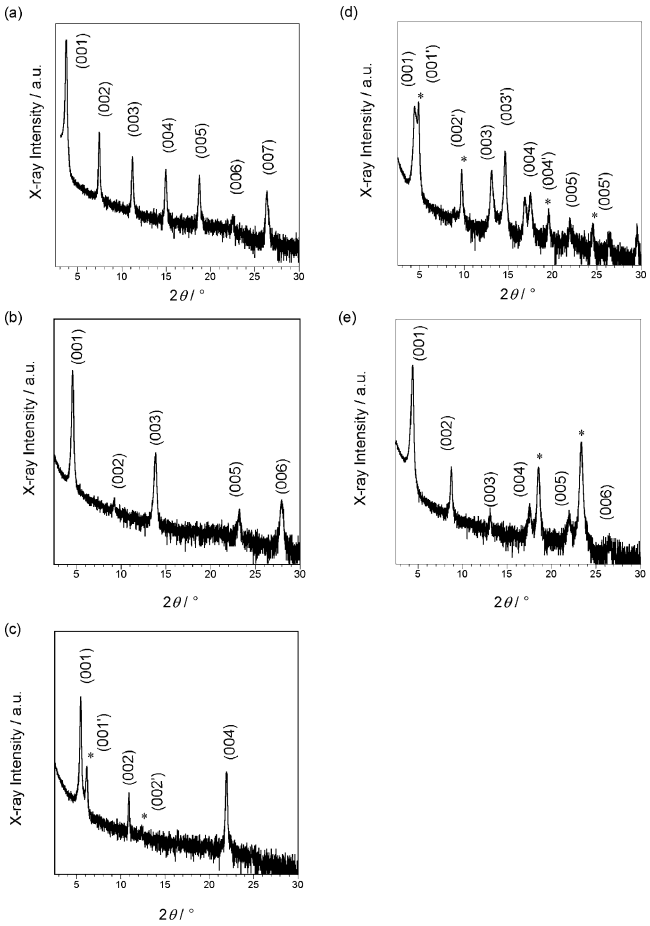

Figure 7. XRDs of evaporated thin film of (a) BHTh−NDT (**2**), (b) BBTh−NDT (**3**), (c) DPh−NDT (**4**), (d) DNap−NDT (**5**), and (e) BBPh−NDT (**6**) (T_{sub} = rt). In the XRDs of **4** and **5** peaks originating from "thin film phase" (00*l*) and "single-crystal phase" (00*l*′) designated with asterisks are observed. The peaks with asterisks in the XRD of **6** cannot be assigned.

Table 4. Interlayer Spacing (*d*), Molecular Lengths (*l*), and Calculated Tilt Angle (θ_{tilt}) for **2**−**6**

	d/Å[a]	molecular length (*l*)/Å[b]	tilt angle (θ_{tilt})/deg[d]
BHTh−NDT (**2**)	23.9	29.6[c]	36
BBTh−NDT (**3**)	19.3	23.5[c]	35
DPh−NDT (**4**)	16.2, 14.4	16.3	6, 28
DNap−NDT (**5**)	20.2, 18.1	20.8	14, 30
BBPh−NDT (**6**)	20.2	24.7	35

[a] Determined on the basis of the first-layer line in the $\theta - 2\theta$ scan of the thin films. [b] Determined on the basis of the single-crystal X-ray structural analysis. [c] Estimated by MOPAC−PM3 calculation. [d] Calculated by $\theta_{tilt} = \cos^{-1}(d/l)$.

two unexplainable peaks at 2θ = 18.53° and 23.33°, indicates a *d* spacing 20.2 Å, resulting in a tilt angle of 35° of the molecules from the normal to the substrate. Although the tilt angles of **3** and **6** are almost the same as that of **2**, the loss of intermolecular π-overlap caused by inclination is compensated for by extension of the π-electron system by the long substituents, and as a result, the FET mobilities of **3** and **6** ($\sim 10^{-2}$ cm^2 V^{-1} s^{-1}) are much improved as compared to that of **2**. The inclined molecular orientations are kept in the films deposited at higher T_{sub} (see Supporting Information for XRDs of **3** and **6** at T_{sub} = 60 and 100 °C), qualitatively agreeing with a small dependence of the mobilities on T_{sub}.

As shown in Figure 7c and d the XRDs of **4** and **5** can be understood by superposition of two series of peaks designated

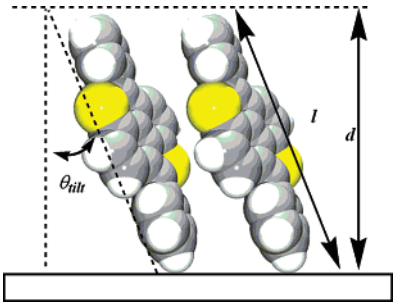

Figure 8. Schematic diagram of the interlayer spacing (d), molecular length (l), and tilt angle of the molecules (θ_{tilt}).

by (00l) and (00l') reflections. This suggests that the films are composed of two kinds of crystal grains with different phases. The large d spacings for **4** and **5** calculated from the (00l) reflections are 16.2 and 20.2 Å, respectively, and very close to the molecular lengths, indicating that the molecules stand nearly upright on the Si/SiO_2 substrate. On the other hand, the small d spacings for **4** and **5** calculated from the (00l') reflections are 14.4 and 18.1 Å, respectively. These values are almost equal to the layer widths in their single-crystal structures (see Figure 2a and b); this means that the molecular arrangements of the phases showing the (00l') reflections are similar to those in single crystals of **4** and **5**. In the discussion below the phase with the (00l) reflections is simply called "thin film phase" whereas that with the (00l') reflections is called "single-crystal phase".

Figure 9 shows XRDs of thin films of **4** and **5** deposited at T_{sub} = 60 and 140 °C. Comparing these diffractograms with those at T_{sub} = rt shown in Figure 7c and d, one can notice that high T_{sub} markedly reduces the proportion of the "single-crystal phase", and only a trace amount of the "single-crystal phase" is detected at T_{sub} = 140 °C. It is evident that the improved FET characteristics of **4** and **5** at high T_{sub} are caused by morphological changes of these thin films to large crystalline grains of "thin film phase" and that carrier migration favorably occurs via the "thin film phase" rather than the "single-crystal phase".

We understand that the low μ_{FET} in the "single-crystal phase" is ascribable to small intermolecular overlap in the molecular arrangement observed in the single-crystal X-ray structures. In contrast, the high μ_{FET} in the "thin film phase" originates from the perpendicular molecular orientation to the substrate, which allows efficient intermolecular charge migration, similar to the case reported for pentacene thin film.[28] In addition, the higher maximum μ_{FET} of **5** than that of **4** may be caused by the larger extension of π-conjugation with naphthalene substituents.

Summary and Conclusions

We successfully developed a series of 2,6-diaryl-NDTs by palladium-catalyzed Suzuki−Miyaura coupling and found that they behave as active materials for p-type OFET devices. Their FET properties depend on the aryl substituents as well as the temperature of the Si/SiO_2 substrate during film deposition, but the mobilities are relatively good and widely range from 10^{-4} to 10^{-1} cm^2 V^{-1} s^{-1}, depending on the substituent groups as well as the fabrication condition of the device. The mobilities of the devices using films of **4** and **5** markedly increase with increasing temperature of the Si/SiO_2 substrate during film deposition. In particular, the device based on the naphthyl derivative **5**, when fabricated at 140 °C, marked a high mobility of 0.11 cm^2 V^{-1} s^{-1} with an on/off ratio of 10^5, which is a top class of performance among recently developed thin film organic

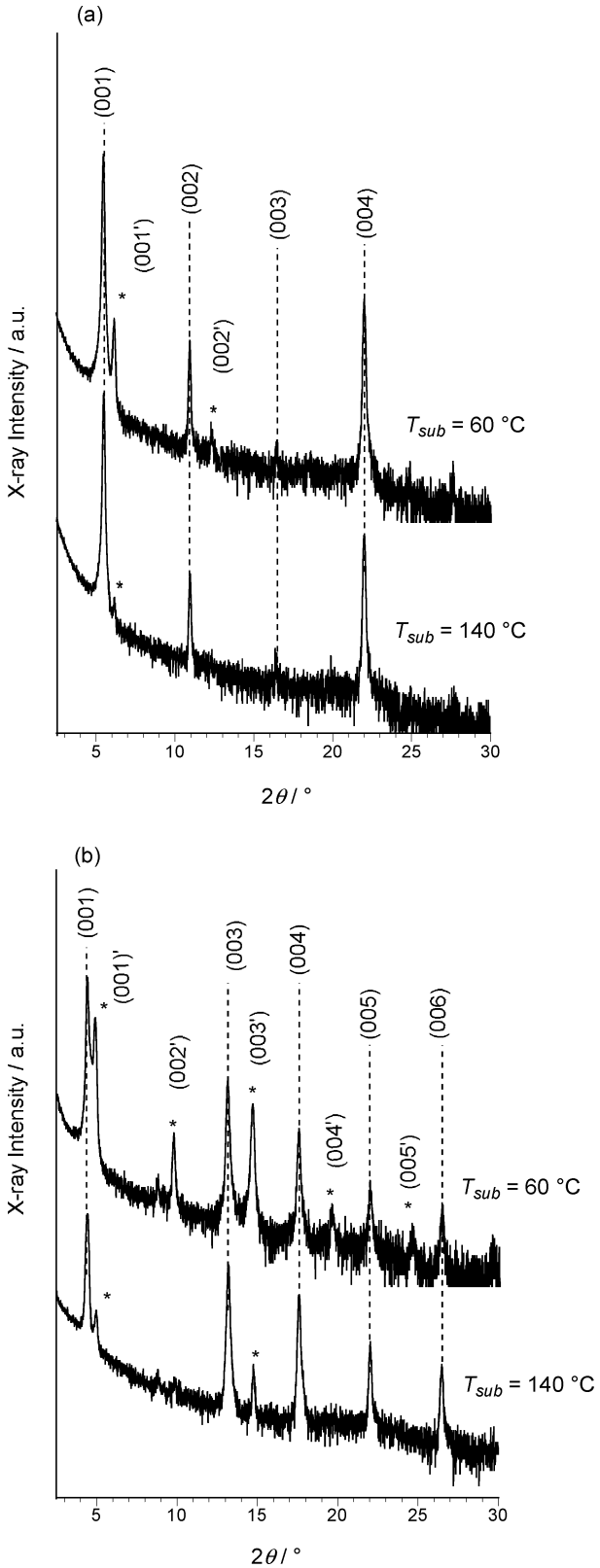

Figure 9. XRDs of thin films evaporated at T_{sub} = 60 and 140 °C: (a) DPh−NDT (**4**) and (b) DNap−NDT (**5**).

(28) Dimitrakopoulos, C. D.; Brown, A. R.; Pomp, A. *J. Appl. Phys.* **1996**, *80*, 2501−2508.

semiconductors. The enhanced FET performances of **4** and **5** at high T_{sub} are ascribable to an increase of large grains with the "thin film phase" in which molecules take a nearly vertical orientation against the substrate. In contrast, the bithiophenyl derivative **3** and the biphenylyl derivative **6**, though they are extended π-conjugated systems favorable for intermolecular charge migration, show lower FET mobilities and on/off ratios as well as a smaller T_{sub} dependence. These are explained by the fact that the molecules in the thin films largely tilt (ca. 35°) from the normal to the substrate.

The present observation of high FET mobilities for all 2,6-diaryl-NDT derivatives strongly indicates that the *anti*-NDT system is notable as a new type for good organic semiconductors. In addition, in this system it is worthy of notice that a subtle structural change of the aryl substituent group results in a drastic change of the molecular orientation in the thin film, which is crucial for FET performance. It is thus strongly suggested that not only the search for prototypical semiconducting molecules but also their systematic structural modifications are required for developing high-performance FET materials.

Acknowledgment. This work was partially supported by the Industrial Technology Research Grant Program in 2004 from the New Energy and Industrial Technology Development Organization (NEDO) of Japan and The Zeneral Oil Research Foundation. K.T. is indebted for financial support from The Nakajima Foundation. We are also grateful to Professor S. Yamanaka (Hiroshima University) for the XRD measurements..

Supporting Information Available: Synthetic details of **2**−**6**, XRDs and AFM images of the thin films of **3** and **6** evaporated at T_{sub} = 60 and 100 °C, crystallographic information files (CIF) for **4**−**6**. This material is available free of charge via the Internet at http://pubs.acs.org.

JA043429P